Published online 20 January 2023

Nucleic Acids Research, 2023, Vol. 51, No. 3 ***1317–1325***
https://doi.org/10.1093/nar/gkac1268

Snapshots of the first-step self-splicing of *Tetrahymena* ribozyme revealed by cryo-EM

Xiaojing Zhang [1,†], Shanshan Li [1,*,†], Grigore Pintilie [2], Michael Z. Palo [3] and Kaiming Zhang [1,*]

[1]Department of Urology, The First Affiliated Hospital of USTC, MOE Key Laboratory for Cellular Dynamics, Division of Life Sciences and Medicine, University of Science and Technology of China, Hefei 230001, China, [2]Department of Bioengineering, Stanford University, Stanford, CA 94305, USA and [3]Department of Biochemistry, Stanford University, Stanford, CA 94305, USA

Received July 01, 2022; Revised December 20, 2022; Editorial Decision December 21, 2022; Accepted January 18, 2023

ABSTRACT

***Tetrahymena* ribozyme is a group I intron, whose self-splicing is the result of two sequential ester-transfer reactions. To understand how it facilitates catalysis in the first self-splicing reaction, we used cryogenic electron microscopy (cryo-EM) to resolve the structures of L-16 *Tetrahymena* ribozyme complexed with a 11-nucleotide 5′-splice site analog substrate. Four conformations were achieved to 4.14, 3.18, 3.09 and 2.98 Å resolutions, respectively, corresponding to different splicing intermediates during the first enzymatic reaction. Comparison of these structures reveals structural alterations, including large conformational changes in IGS/IGSext (P1-P1ext duplex) and J5/4, as well as subtle local rearrangements in the G-binding site. These structural changes are required for the enzymatic activity of the *Tetrahymena* ribozyme. Our study demonstrates the ability of cryo-EM to capture dynamic RNA structural changes, ushering in a new era in the analysis of RNA structure-function by cryo-EM.**

INTRODUCTION

RNA research is currently one of the most rapidly developing hotspots and frontiers of life science research in the world. Studies on the structures and functional mechanisms of RNAs play a crucial role in our understanding of the biochemical principles essential for life and the occurrence of diseases. RNA primary sequences form relatively stable secondary structures through base pairing, and then fold into more complex three-dimensional structures through long-distance interactions, performing various regulatory and catalytic functions (1–3). How the structures of RNAs change dynamically in biological processes and then exert their regulatory functions is an important scientific problem to be solved urgently.

Tetrahymena thermophila ribozyme is the first RNA with enzymatic activity that does not involve protein, discovered by Thomas Cech (4). It is a group I intron, whose self-splicing is the result of two sequential transesterification reactions (5). The presence of metal ions, especially Mg^{2+}, is essential for the stability of the RNA structure and catalytic reaction (6–12). Although structural and functional studies of *Tetrahymena* ribozyme have been extensively performed (13–24), the structural mechanism of the entire self-splicing reaction is still lacking, which leads to uncertainties explaining the biochemical and functional data of this ribozyme, limiting its application as a gene regulation tool in molecular therapy and RNA nanotechnology (3).

Here, taking advantage of single-particle cryogenic electron microscopy (cryo-EM) to resolve samples of high heterogeneity or flexibility (25,26), we obtained the high-resolution three-dimensional (3D) structures of four functional states of *Tetrahymena* ribozyme during the first-step self-splicing. These structures allow us to understand how conformational changes promote catalysis, providing direct structural insights into the mechanism of this model ribozyme and promote its practical applications.

MATERIALS AND METHODS

RNA sample preparation

The *Tetrahymena* ribozyme RNA sample was produced as previously stated (16). The forward primer 5′-TAATACGACTCACTATAGGTTTGGAGG GAAAAGTTATCA-3′ and the reverse primer 5′-(MeA)(MeC)TCCAAAACTAATCAATATACTTT-3′ were used to amplify the DNA template from the pUC57-16 plasmid. ‘Me’ stands for the methoxyl modification, which was added to ensure the integrity and precision of

*To whom correspondence should be addressed. Tel: +86 13694415677; Email: kmzhang@ustc.edu.cn
Correspondence may also be addressed to Shanshan Li. Tel: +86 13404537768; Email: lishanshan@ustc.edu.cn
†The authors wish it to be known that, in their opinion, the first two authors should be regarded as Joint First Authors.

the transcribed RNA 3′-end sequence. *In vitro* transcription reaction was performed in a mixture comprising 0.315 μM DNA template, 40 mM Tris, pH 7.9, 20 mM $MgCl_2$, 2 mM spermidine, 0.01% Triton X-100, 4 mM DTT, 2 mM NTPs, 1 U/μl recombinant ribonuclease inhibitor (TaKaRa), and 7 mg/ml laboratory-purified T7 RNA polymerase for 4 h at 37°C. The resultant RNA was loaded and run on an 8% urea–PAGE gel, and target RNA was extracted from the gel by spinning overnight at 4°C with a binding buffer containing 300 mM NaOAc, pH 5.2, 1 mM EDTA. Then RNA was purified by isopropanol precipitation and finally dissolved in RNase-free water. The RNA oligonucleotide substrates (5′-FAM-cccucu*aaacc3′ or 5′cccucu*aaacc3′), in which * indicates a phosphorothioate bond, were acquired from Accurate Biotechnology (Hunan) Co., Ltd. FAM refers to 6-Carboxyfluorescein (6-FAM), single isomer.

First-step self-splicing reaction assay

Three different concentrations (1, 2, 3 μM) of ribozyme RNA were refolded in a buffer containing 50 mM Na-HEPES, pH 8 as follows: denaturation at 90°C for 3 min, cooling to room temperature (RT) for 10 min, addition of 10 mM $MgCl_2$ and incubation at 50°C for 30 min, as well as cooling again to RT for 10 min. Then, 1 mM GTP was added to the RNA samples for another 5 min. The FAM-labeled substrate (1 μM final concentration) was added and incubated at RT for 20 min to form holoenzyme complexes, followed by incubation on ice for another 2 h. Samples were loaded onto a 20% urea–PAGE gel and run at 180 V for 80 min, and imaged using the fluorescence imaging system Typhoon FLA 7000 (General Electric).

Cryo-EM sample preparation

To prepare the *Tetrahymena* ribozyme sample for cryo-EM analysis, the concentrations of ribozyme and substrate RNAs were increased. Briefly, ∼20 μM ribozyme was refolded, and 1 mM GTP was added and incubated at RT for 5 min. Then, 75 μM of the substrate without the FAM label was added and incubated at RT for 20 min to form holoenzyme complexes, followed by an additional 2 h on ice. Three microliters of the *Tetrahymena* ribozyme sample were applied onto glow-discharged 200-mesh R2/1 Quantifoil copper grids. The grids were blotted for 4 s and rapidly cryocooled in liquid ethane using a Vitrobot Mark IV (Thermo Fisher Scientific) at 4°C and ∼100% humidity.

Cryo-EM data collection

The grids were screened using a Talos Glacios cryo-electron microscope (Thermo Fisher Scientific) operated at 200 kV. The grids were imaged in a Titan Krios cryo-electron microscope (Thermo Fisher Scientific) operated at 300 kV at a magnification of 105 000× (corresponding to a calibrated sampling of 0.82 Å per pixel). Micrographs were recorded by EPU software (Thermo Fisher Scientific) with a Gatan K3 Summit direct electron detector, where each image was composed of 30 individual frames with an exposure time of 3 s and a dose rate of 17 electrons per second per $Å^2$. Finally, a total of 18 241 movie stacks were collected with a defocus range of −0.8 to −2.8 μm.

Image processing

All micrographs were motion-corrected using MotionCor2 (27) and the contrast transfer function (CTF) was determined using CTFFIND4 (28). All particles were autopicked using the NeuralNet option in EMAN2 (29) and further checked manually. The resulting number of boxed particles was 3 668 247. Then, particle coordinates were imported to Relion (30), where three rounds of 2D classification were performed to remove 2D class averages with less resolved features. The selected 1 644 225 particles were imported to cryoSPARC (31) for generating ab-initio maps, and two good conformations with a discernible difference in the 5′-end of the intron were derived. Then starting with the two conformations, we performed the Non-Uniform Refinement together with Local and Global CTF Refinement, yielding two maps with 3.26-Å resolution from 350 220 particles and 3.10-Å resolution from 524 508 particles. Further heterogeneous refinement was performed to classify slightly different conformations in each of the above two classes, and totally four conformations were obtained. Final maps were achieved after another round of Non-uniform Refinement for each of the four classes, with resolutions at 4.14, 3.18, 3.09 and 2.98 Å, respectively. The cited resolutions for the final maps were estimated by the 0.143 criterion of FSC curve in cryoSPARC. (See more information in Supplementary Figure S2 and Supplementary Table S1).

Model building

We applied auto-DRRAFTER (32), an RNA-specific modeling tool, to build the initial models for these maps. The atomic model of full-length holo *Tetrahymena* ribozyme (PDB ID: 7EZ2) was first rigidly fitted into the cryo-EM densities of Con1–4. Two rounds of modeling were performed for each conformation. Then the top-scoring models of Con1–4 were subjected to model optimization with Coot (33). The resultant models were refined using phenix.real_space_refine with secondary structure and geometry restraints (34). The quality of final models was evaluated by MolProbity (35). Statistics of the map reconstruction and model optimization are summarized in Supplementary Table S1. All figures were made using Chimera (36) or ChimeraX (37).

RESULTS

Cryo-EM structures of multiple states from the first-step self-splicing of *Tetrahymena* ribozyme

To dissect the structural rearrangements in the self-splicing process, we used the internal guide sequence extension (IGSext)-containing ribozyme, *Tetrahymena* L-16 ScaI ribozyme. It has the ability to form dynamic helices involved in substrate recognition during self-splicing, including the P1 extension (P1ext) at the 5′-splice site and P10 at the 3′-splice site (24). To mimic the first-step self-splicing

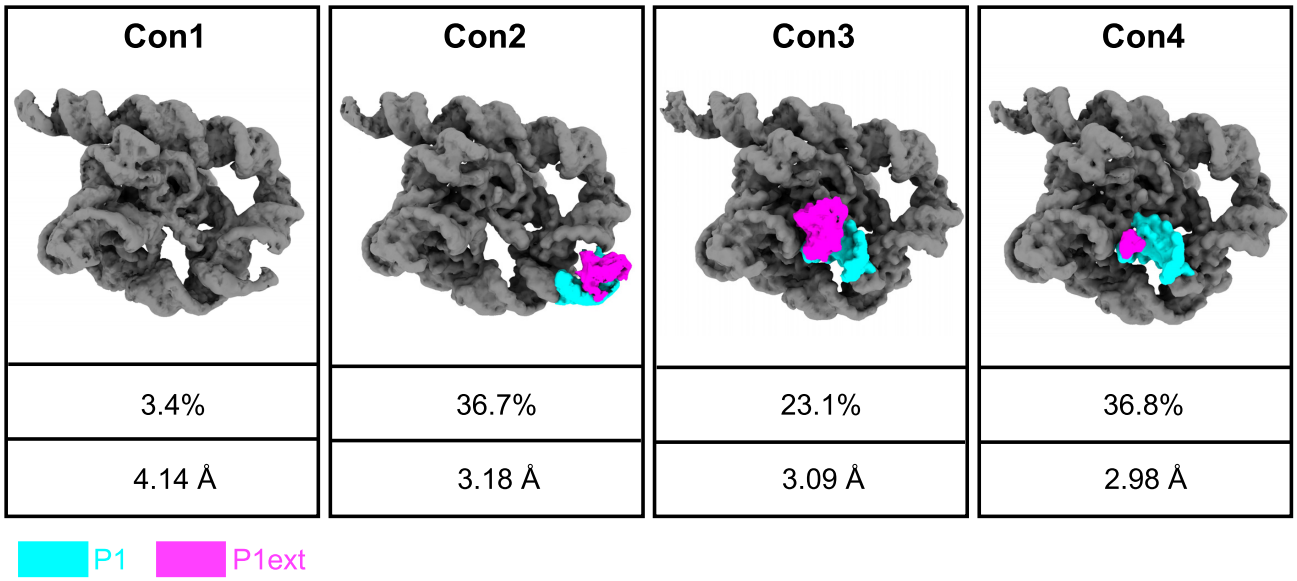

Figure 1. Different states (Con1–4) from the first-step self-splicing of *Tetrahymena* ribozyme resolved by cryo-EM. The percentages and resolutions in the last two rows refer to the final dataset and final maps.

of the L-16 ScaI ribozyme, 5′-splice site analog substrate (5′cccucu*aaacc3′) and exogenous G (exoG) were added. The scissile phosphodiester bond in the substrate was substituted to the phosphorothioate bond (*) to slow down the cleavage reaction, giving us the opportunity to capture multiple conformations for the first step of self-splicing.

We first validated the catalytic ability of the ribozyme using an *in vitro* splicing assay (Supplementary Figure S1A). After sample screening, we collected a large dataset of 18 241 movie stacks to obtain sufficient ribozyme particles to classify different splicing states. During image processing, two recognizable conformations with a distinct difference at the 5′-end were obtained from Ab-initio 3D reconstruction and refinement in CryoSPARC (Supplementary Figures S1B, C and S2). Further 3D classification resolved four distinct conformations, which accounted for 3.4%, 36.7%, 23.1% and 36.8% of the total particles, respectively. These maps were further refined to 4.14, 3.18, 3.09 and 2.98 Å, respectively (Supplementary Figure S3). These resolutions allow us to determine the atomically detailed structures of *Tetrahymena* ribozyme, revealing the structural basis for how it facilitates catalysis. Hereafter, we refer to these four structures as Con1, Con2, Con3, and Con4, according to the order in which they may appear during self-splicing (Figure 1).

Structural features of the apoenzyme and undocked forms of *Tetrahymena* ribozyme

Con1 and Con2 have an unbent 5′-end, indicating that they are in a pre-docking state. In Con1, the single-stranded IGS can be resolved (Figure 2A, Supplementary Figure S4A, and Movie S1). In contrast, the P1-P1ext helix formed by substrate and IGS/IGSext can be observed in Con2 (Figure 2B) (38–40). Comparisons between Con1 and Con2 show that the main difference is at the 5′-end of the intron, with negligible change to the catalytic core (Figure 2C). We therefore conclude that in Con1 and Con2, the oligonucleotide substrate base pairs with the apoenzyme to form the P1-P1ext duplex. Oligonucleotide substrate binding and exoG binding have been reported to be independent (17). In these two pre-docking states, GTP (exoG) can already be resolved well (Figure 2A and B). The exoG binding precedes duplex docking may be due to exoG being necessary for duplex docking (20,41) or faster exoG binding (concentration ratio$_{exoG/oligo}$ > 10-fold in our sample).

Structural features of the pre-catalysis and post-catalysis states of *Tetrahymena* ribozyme

Compared with Con2, the 5′-terminal duplex of Con3 containing the substrate undergoes a 53-Å distance movement to dock into the intron's active site (Supplementary Figure S4B and Movie S1). Tertiary interactions between P1 and three single-stranded segments within the catalytic core (J8/7, J4/5, J5/4) mediate docking of the P1-P1ext duplex into the active site. These include interactions between the catalytic core and the substrate at residues a(+1) - u(−3) and between the catalytic core and the IGS at residues G22–23, G25–27 (Supplementary Figure S4C). A tertiary interaction involving A29 and the first base pair A31–U56 in helix P2 stabilizes the P1-P1ext docked state (Figure 3A) (42). The last base pair of P1 is the U•G wobble that has been shown to specify the 5′-splice site (43,44). The U defines the 3′-end of the 5′-exon, and the complementary G is part of the IGS base-paired to the 5′-exon. The minor groove surface of the U•G wobble is recognized by A207 and A114, helping to pack the helix against J4/5 (Figure 3A) (45). A similar recognition scheme is also adopted by the *Azoarcus* intron (43). The distance between the 3′-OH group of the G nucleophile and the scissile phosphorus is 3.11 Å (Figure 3A), therefore, Con3 is the conformation ready for the first transesterification reaction.

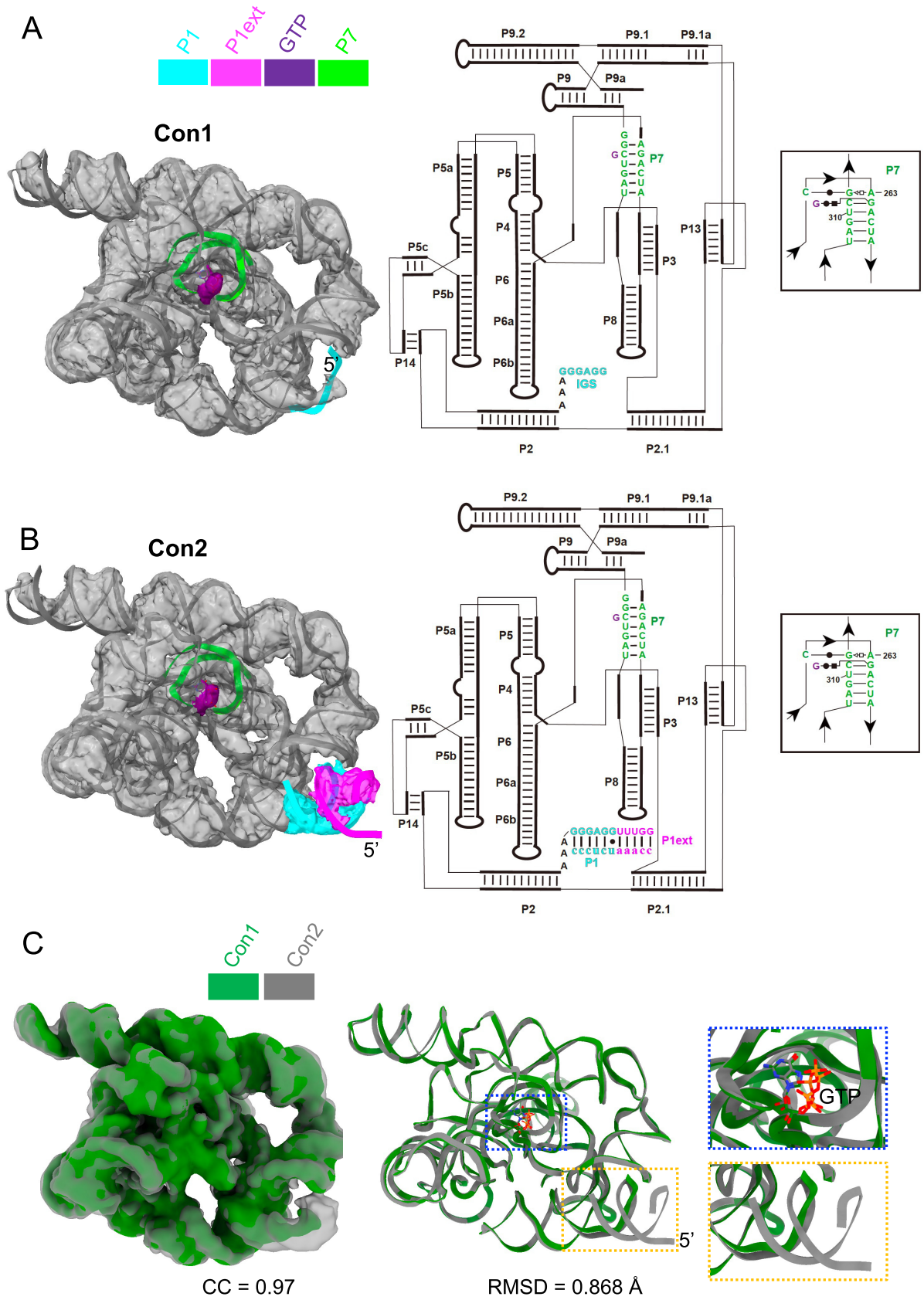

Figure 2. Structural features of *Tetrahymena* ribozyme in Con1 and Con2. (A, B) Cryo-EM maps, models, and secondary structures of Con1 (**A**) and Con2 (**B**). The oligonucleotide substrate sequence is shown in lowercase and ribozyme sequence is shown in UPPERCASE. (**C**) Superpositions of Con1 and 2. Blue and orange boxes illustrate the catalytic core and 5′-end of the intron, respectively. GTP is colored by heteroatom for highlighting.

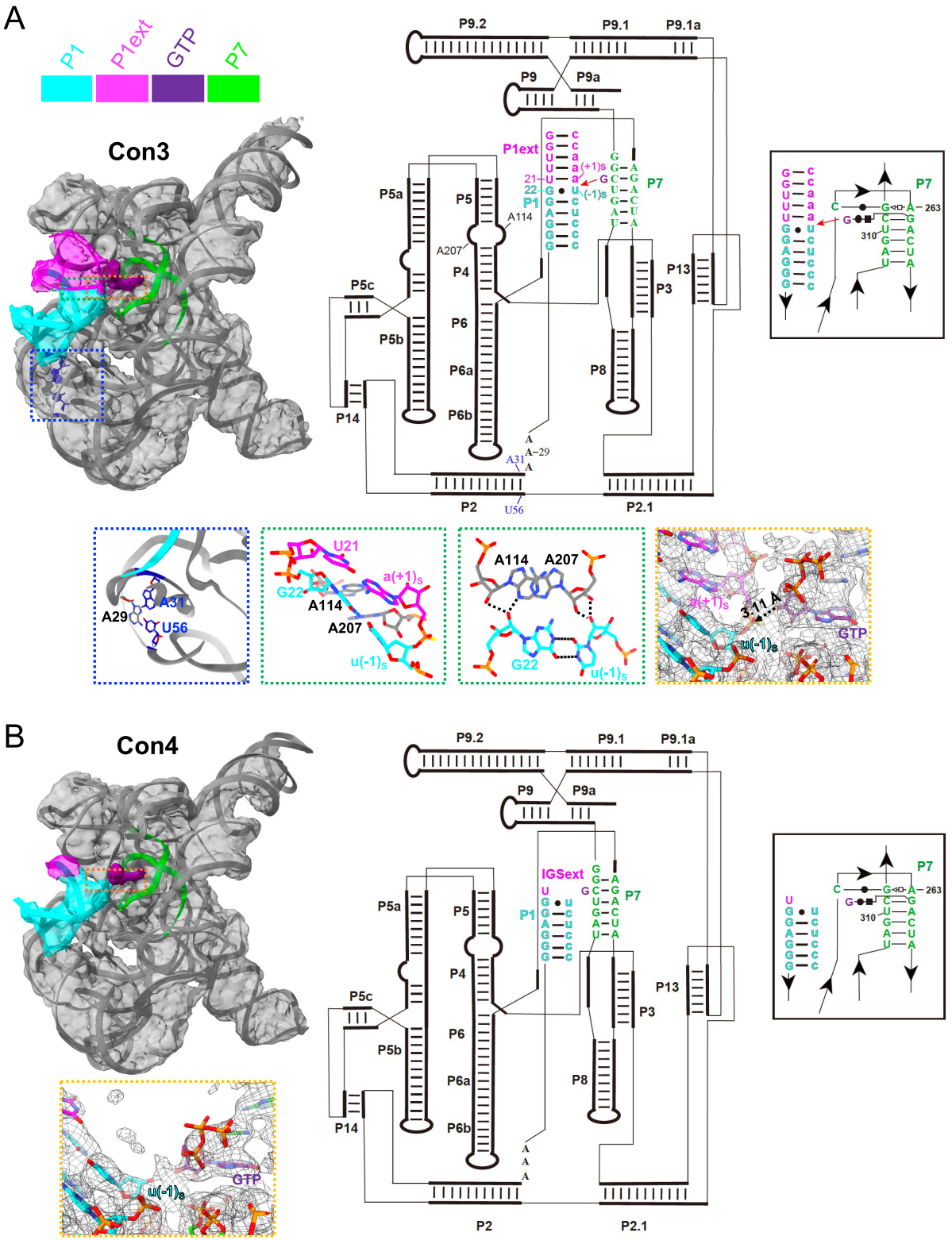

Figure 3. Structural features of *Tetrahymena* ribozyme in Con3 and Con4. (**A**) Cryo-EM map, model, and secondary structure of Con3. Blue box highlights a tertiary interaction (A29–A31–U56) stabilizing the docked duplex. Green box shows a helix packing at the 5′-splice site, and hydrogen bonds are indicated as black dashed lines. Orange box is the zoom-in view of the active site, where the nucleophilic attack will occur. (**B**) Cryo-EM map, model, and secondary structure of Con4. Orange box is the zoom-in view of the active site, where the nucleophilic attack has been accomplished.

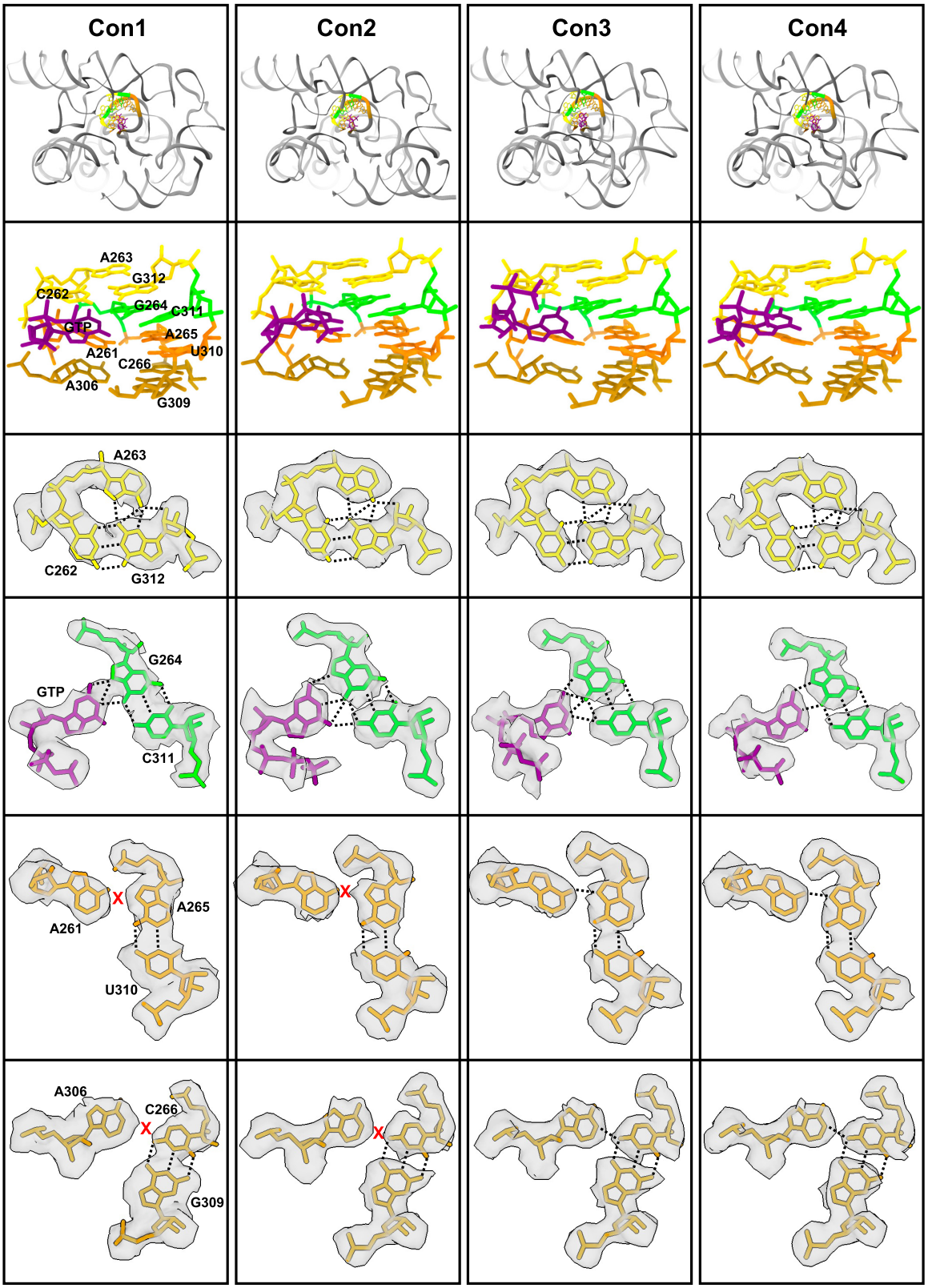

Figure 4. Comparison of G-binding sites among different conformations. Different base triples in the active site are shown in different colors. The base triple interactions are indicated as black dashed lines. The symbol 'X' in red color refers to loss of base triple interactions.

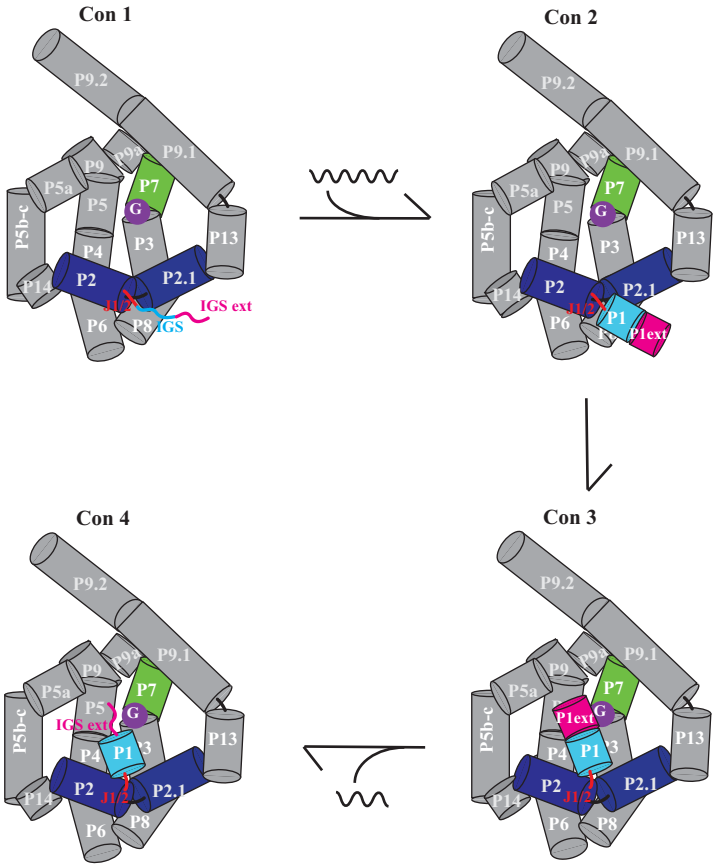

Figure 5. Schematic representation of *Tetrahymena* ribozyme during the first-step self-splicing. P denotes paired regions, and J denotes junctions connecting paired regions. The wavy line indicates the oligonucleotide substrate or product.

Con4 shares the same overall architecture with Con3, except the absence of the P1ext helix (Figure 3B and Movie S1), suggesting that Con4 has accomplished the first transesterification reaction. Previous kinetic studies of the *Tetrahymena* ribozyme showed that the release of the product oligonucleotide in the first step of self-splicing is very slow (17,18). This rate-limiting step allows us to capture Con4, occupying the majority of total particles (Figure 1). Notably, we observed the docking of another exoG at the G-binding site (Figure 3B and Movie S1), consistent with the ability of *Tetrahymena* ribozyme to undergo multi-turnover reactions (46–48).

Comparisons of G-binding sites between different splicing states

Previous studies demonstrated that *Tetrahymena* ribozyme has a pre-organized active site (14,16). However, although the overall structure of the active site is close to its active conformation, local rearrangements of the active site may be still needed during enzyme reaction. Superimposing atomic models of the active site from different conformations reveals differences in the IGS/IGSext (P1-P1ext duplex) and J5/4, which are most pronounced between Con2 and Con3 (Supplementary Figure S5). Specifically, the P1-P1ext duplex docks into the active site after base pairing; the movement of J5/4 close to the active site could create a compact environment that may promote catalysis. The exoG forms a major-groove base triple with the G264–C311 pair, as does the 3′-terminal G (ωG) (15,16). As reported, the ωG–G264–C311 triple could be sandwiched by three other layers of base triples (A263–C262–G312, A261–A265–U310, A306–C266–G309). However, A261–A265–U310 and A306–C266–G309 base triples are not formed in Con1-2, but in Con3–4 (Figure 4). This finding indicates that ribozyme binds tightly to the G to facilitate the first ester-transfer reaction and is expected to loosen the active site for the next enzymatic reaction, which is also indicated by previous biochemical studies (49,50). Therefore, large conformational changes as well as subtle local rearrangements are required for the enzymatic activity of *Tetrahymena* ribozyme.

DISCUSSION

The biological functions of RNA molecules often require conformational changes. During the self-splicing process of *Tetrahymena* ribozyme, conformational changes occur upon binding of the substrate or nucleophile (51). In our study, following the addition of the G nucleophile, the first-step self-splicing was observed in three steps (Figure 5): substrate base pairing with the ribozyme to form the P1-P1ext helix, subsequent docking of the P1-P1ext helix into the catalytic core, and the post-docking chemical step. Our

structures explain previous biochemical findings predicting that upon addition of exoG, 5′-exon binding will occur in two steps (38–41). During the above process, large conformational changes involving IGS/IGSext (P1-P1ext duplex) and J5/4 were observed. Subtle local rearrangements were also found, forming a base triple sandwich. These structural alterations create a compact environment conducive to catalysis. As a metalloenzyme, the group I intron requires metal ions (M_A–M_E, M_2) for its folding and catalysis (6–12,16). M_A, M_E and M_2 were found in our high-resolution maps (Con2–4). However, as there were no noticeable changes in metal ions when comparing different conformations, metal ions were not emphasized in this study.

Su *et al.* (16) recently reported cryo-EM structures of the apo L-21 and holo L-16 *Tetrahymena* ribozyme. Notably, a single holo state at the pre-catalysis state during the second self-splicing reaction was captured using the 5′-exon analog (5′cccucu3′) and 3′-splice site analog (5′ucg*uaacc3′) as substrates. Our continuous four structures well complete this previous study and clearly show a detailed structural and mechanistic view of *Tetrahymena* ribozyme undergoing the first self-splicing reaction (Supplementary Figure S6).

In addition to the conformational changes captured in this work and previous study (16), structural changes related to two aspects of the self-splicing process are still under investigation, namely how the ribozyme reorganizes itself from the first to the second transesterification reaction and how the ligated substrate is released (Supplementary Figure S6). Our study highlights the ability of cryo-EM to capture dynamic RNA structural changes, opening a new era of RNA structure–function analysis by cryo-EM.

DATA AVAILABILITY

Cryo-EM structures and atomic models have been deposited in the wwPDB OneDep System under EMD accession codes EMD-33736, EMD-33738, EMD-33739, EMD-33740 and PDB ID codes under accession codes 7YC8, 7YCG, 7YCH, 7YCI, respectively.

SUPPLEMENTARY DATA

Supplementary Data are available at NAR Online.

ACKNOWLEDGEMENTS

We thank the Cryo-EM Center at University of Science and Technology of China for the support of cryo-EM data collection.

Author contributions. K.Z. and S.L. conceived the study and designed the experiments. X.Z. prepared the RNA samples. X.Z. and K.Z. performed cryo-EM sample preparation, screening, and data collection. S.L., X.Z. and K.Z. performed image processing and structure determination. S.L. built and refined the models. G.P. made the movie. X.Z., S.L., M.P., K.Z. and G.P. analyzed the data. S.L. and K.Z. wrote and edited the manuscript with input from all other authors.

FUNDING

Ministry of Science and Technology of China [MoST 2022YFC2303700 to K.Z., S.L., 2022YFA1302700 to K.Z.]; start-up funding from University of Science and Technology of China [KY9100000032, KJ2070000080 to K.Z.]; Fundamental Research Funds for the Central Universities [WK9100000044 to K.Z.]. Funding for open access charge: University of Science and Technology of China.
Conflict of interest statement. None declared.

REFERENCES

1. Wilson,T.J., Liu,Y. and Lilley,D.M.J. (2016) Ribozymes and the mechanisms that underlie RNA catalysis. *Front. Chem. Sci. Eng.*, **10**, 178–185.
2. Jimenez,R.M., Polanco,J.A. and Lupták,A. (2015) Chemistry and biology of self-cleaving ribozymes. *Trends Biochem. Sci.*, **40**, 648–661.
3. Müller,S., Appel,B., Balke,D., Hieronymus,R. and Nübel,C. (2016) Thirty-five years of research into ribozymes and nucleic acid catalysis: where do we stand today?*F1000Res.*, **5**, F1000 Faculty Rev-1511.
4. Kruger,K., Grabowski,P.J., Zaug,A.J., Sands,J., Gottschling,D.E. and Cech,T.R. (1982) Self-splicing RNA: autoexcision and autocyclization of the ribosomal RNA intervening sequence of Tetrahymena. *Cell*, **31**, 147–157.
5. Cech,T.R. (1990) Self-splicing of group I Introns. *Annu. Rev. Biochem.*, **59**, 543–568.
6. Piccirilli,J.A., Vyle,J.S., Caruthers,M.H. and Cech,T.R. (1993) Metal ion catalysis in the Tetrahymena ribozyme reaction. *Nature*, **361**, 85–88.
7. Weinstein,L.B., Jones,B.C.N., Cosstick,R. and Cech,T.R. (1997) A second catalytic metal ion in a group I ribozyme. *Nature*, **388**, 805–808.
8. Shan,S.-O., Kravchuk,A.V., Piccirilli,J.A. and Herschlag,D. (2001) Defining the catalytic metal ion interactions in the Tetrahymena ribozyme reaction†. *Biochemistry*, **40**, 5161–5171.
9. Yoshida,A., Sun,S. and Piccirilli,J.A. (1999) A new metal ion interaction in the Tetrahymena ribozyme reaction revealed by double sulfur substitution. *Nat. Struct. Biol.*, **6**, 318–321.
10. Sjogren,A. (1997) Metal ion interaction with cosubstrate in self-splicing of group I introns. *Nucleic Acids Res.*, **25**, 648–653.
11. Forconi,M., Piccirilli,J.A. and Herschlag,D. (2007) Modulation of individual steps in group I intron catalysis by a peripheral metal ion. *RNA*, **13**, 1656–1667.
12. Shan,S.O. and Herschlag,D. (2000) An unconventional origin of metal-ion rescue and inhibition in the Tetrahymena group I ribozyme reaction. *RNA*, **6**, 795–813.
13. Cate,J.H., Gooding,A.R., Podell,E., Zhou,K., Golden,B.L., Kundrot,C.E., Cech,T.R. and Doudna,J.A. (1996) Crystal structure of a group I ribozyme domain: principles of RNA packing. *Science*, **273**, 1678–1685.
14. Golden,B.L., Gooding,A.R., Podell,E.R. and Cech,T.R. (1998) A preorganized active site in the crystal structure of the Tetrahymena ribozyme. *Science*, **282**, 259–264.
15. Guo,F., Gooding,A.R. and Cech,T.R. (2004) Structure of the Tetrahymena ribozyme: base triple sandwich and metal ion at the active site. *Mol. Cell*, **16**, 351–362.
16. Su,Z., Zhang,K., Kappel,K., Li,S., Palo,M.Z., Pintilie,G.D., Rangan,R., Luo,B., Wei,Y., Das,R. *et al.* (2021) Cryo-EM structures of full-length Tetrahymena ribozyme at 3.1 Å resolution. *Nature*, **596**, 603–607.
17. Herschlag,D. and Cech,T.R. (1990) Catalysis of RNA cleavage by the Tetrahymena thermophila ribozyme. 1. Kinetic description of the reaction of an RNA substrate complementary to the active site. *Biochemistry*, **29**, 10159–10171.
18. Herschlag,D. and Cech,T.R. (1990) Catalysis of RNA cleavage by the Tetrahymena thermophila ribozyme. 2. Kinetic description of the reaction of an RNA substrate that forms a mismatch at the active site. *Biochemistry*, **29**, 10172–10180.
19. Karbstein,K., Carroll,K.S. and Herschlag,D. (2002) Probing the Tetrahymena group I ribozyme reaction in both directions. *Biochemistry*, **41**, 11171–11183.

20. Bevilacqua,P.C., Kierzek,R., Johnson,K.A. and Turner,D.H. (1992) Dynamics of ribozyme binding of substrate revealed by fluorescence-detected stopped-flow methods. *Science*, **258**, 1355–1358.
21. Pyle,A.M., McSwiggen,J.A. and Cech,T.R. (1990) Direct measurement of oligonucleotide substrate binding to wild-type and mutant ribozymes from Tetrahymena. *Proc. Natl. Acad. Sci. U.S.A.*, **87**, 8187–8191.
22. Karbstein,K. and Herschlag,D. (2003) Extraordinarily slow binding of guanosine to the Tetrahymena group I ribozyme: implications for RNA preorganization and function. *Proc. Natl. Acad. Sci. U.S.A.*, **100**, 2300–2305.
23. Zarrinkar,P.P. and Sullenger,B.A. (1998) Probing the interplay between the two steps of group I intron splicing: competition of exogenous guanosine with omega G. *Biochemistry*, **37**, 18056–18063.
24. Karbstein,K., Lee,J. and Herschlag,D. (2007) Probing the role of a secondary structure element at the 5′- and 3′-splice sites in group I intron self-splicing: the tetrahymena L-16 ScaI ribozyme reveals a new role of the G.U pair in self-splicing. *Biochemistry*, **46**, 4861–4875.
25. Zhang,K., Zhang,H., Li,S., Pintilie,G.D., Mou,T.-C., Gao,Y., Zhang,Q., van den Bedem,H., Schmid,M.F., Au,S.W.N. *et al.* (2019) Cryo-EM structures of vacuolating cytotoxin A oligomeric assemblies at near-atomic resolution. *Proc. Natl. Acad. Sci. U.S.A.*, **116**, 6800–6805.
26. Ma,H., Jia,X., Zhang,K. and Su,Z. (2022) Cryo-EM advances in RNA structure determination. *Signal Transduct. Target. Ther.*, **7**, 58.
27. Zheng,S.Q., Palovcak,E., Armache,J.-P., Verba,K.A., Cheng,Y. and Agard,D.A. (2017) MotionCor2: anisotropic correction of beam-induced motion for improved cryo-electron microscopy. *Nat. Methods*, **14**, 331–332.
28. Rohou,A. and Grigorieff,N. (2015) CTFFIND4: fast and accurate defocus estimation from electron micrographs. *J. Struct. Biol.*, **192**, 216–221.
29. Tang,G., Peng,L., Baldwin,P.R., Mann,D.S., Jiang,W., Rees,I. and Ludtke,S.J. (2007) EMAN2: an extensible image processing suite for electron microscopy. *J. Struct. Biol.*, **157**, 38–46.
30. Scheres,S.H.W. (2012) RELION: implementation of a Bayesian approach to cryo-EM structure determination. *J. Struct. Biol.*, **180**, 519–530.
31. Punjani,A., Rubinstein,J.L., Fleet,D.J. and Brubaker,M.A. (2017) cryoSPARC: algorithms for rapid unsupervised cryo-EM structure determination. *Nat. Methods*, **14**, 290–296.
32. Kappel,K., Zhang,K., Su,Z., Watkins,A.M., Kladwang,W., Li,S., Pintilie,G., Topkar,V.V., Rangan,R., Zheludev,I.N. *et al.* (2020) Accelerated cryo-EM-guided determination of three-dimensional RNA-only structures. *Nat. Methods*, **17**, 699–707.
33. Emsley,P., Lohkamp,B., Scott,W.G. and Cowtan,K. (2010) Features and development of Coot. *Acta Crystallogr. D Biol. Crystallogr.*, **66**, 486–501.
34. Adams,P.D., Afonine,P.V., Bunkóczi,G., Chen,V.B., Davis,I.W., Echols,N., Headd,J.J., Hung,L.-W., Kapral,G.J., Grosse-Kunstleve,R.W. *et al.* (2010) PHENIX: a comprehensive Python-based system for macromolecular structure solution. *Acta Crystallogr. D Biol. Crystallogr.*, **66**, 213–221.
35. Chen,V.B., Arendall,W.B. 3rd, Headd,J.J., Keedy,D.A., Immormino,R.M., Kapral,G.J., Murray,L.W., Richardson,J.S. and Richardson,D.C. (2010) MolProbity: all-atom structure validation for macromolecular crystallography. *Acta Crystallogr. D Biol. Crystallogr.*, **66**, 12–21.
36. Pettersen,E.F., Goddard,T.D., Huang,C.C., Couch,G.S., Greenblatt,D.M., Meng,E.C. and Ferrin,T.E. (2004) UCSF Chimera–a visualization system for exploratory research and analysis. *J. Comput. Chem.*, **25**, 1605–1612.
37. Pettersen,E.F., Goddard,T.D., Huang,C.C., Meng,E.C., Couch,G.S., Croll,T.I., Morris,J.H. and Ferrin,T.E. (2021) UCSF ChimeraX: structure visualization for researchers, educators, and developers. *Protein Sci.*, **30**, 70–82.
38. Narlikar,G.J., Bartley,L.E. and Herschlag,D. (2000) Use of duplex rigidity for stability and specificity in RNA tertiary structure. *Biochemistry*, **39**, 6183–6189.
39. Wang,J.F., Downs,W.D. and Cech,T.R. (1993) Movement of the guide sequence during RNA catalysis by a group I ribozyme. *Science*, **260**, 504–508.
40. Campbell,T.B. and Cech,T.R. (1996) Mutations in the Tetrahymena ribozyme internal guide sequence: effects on docking of the P1 helix into the catalytic core and correlation with catalytic activity. *Biochemistry*, **35**, 11493–11502.
41. Bevilacqua,P.C., Li,Y. and Turner,D.H. (1994) Fluorescence-detected stopped flow with a pyrene labeled substrate reveals that guanosine facilitates docking of the 5′ cleavage site into a high free energy binding mode in the Tetrahymena ribozyme. *Biochemistry*, **33**, 11340–11348.
42. Shi,X., Solomatin,S.V. and Herschlag,D. (2012) A role for a single-stranded junction in RNA binding and specificity by the Tetrahymena group I ribozyme. *J. Am. Chem. Soc.*, **134**, 1910–1913.
43. Adams,P.L., Stahley,M.R., Kosek,A.B., Wang,J. and Strobel,S.A. (2004) Crystal structure of a self-splicing group I intron with both exons. *Nature*, **430**, 45–50.
44. Knitt,D.S., Narlikar,G.J. and Herschlag,D. (1994) Dissection of the role of the conserved G.U pair in group I RNA self-splicing. *Biochemistry*, **33**, 13864–13879.
45. Strobel,S.A., Ortoleva-Donnelly,L., Ryder,S.P., Cate,J.H. and Moncoeur,E. (1998) Complementary sets of noncanonical base pairs mediate RNA helix packing in the group I intron active site. *Nat. Struct. Biol.*, **5**, 60–66.
46. Zaug,A.J. and Cech,T.R. (1986) The Tetrahymena intervening sequence ribonucleic acid enzyme is a phosphotransferase and an acid phosphatase. *Biochemistry*, **25**, 4478–4482.
47. Zaug,A.J. and Cech,T.R. (1986) The intervening sequence RNA of Tetrahymena is an enzyme. *Science*, **231**, 470–475.
48. Zaug,A.J., Grosshans,C.A. and Cech,T.R. (1988) Sequence-specific endoribonuclease activity of the Tetrahymena ribozyme: enhanced cleavage of certain oligonucleotide substrates that form mismatched ribozyme-substrate complexes. *Biochemistry*, **27**, 8924–8931.
49. McConnell,T.S., Cech,T.R. and Herschlag,D. (1993) Guanosine binding to the Tetrahymena ribozyme: thermodynamic coupling with oligonucleotide binding. *Proc. Natl. Acad. Sci. U.S.A.*, **90**, 8362–8366.
50. Bao,P., Wu,Q.-J., Yin,P., Jiang,Y., Wang,X., Xie,M.-H., Sun,T., Huang,L., Mo,D.-D. and Zhang,Y. (2008) Coordination of two sequential ester-transfer reactions: exogenous guanosine binding promotes the subsequent omegaG binding to a group I intron. *Nucleic Acids Res.*, **36**, 6934–6943.
51. Shan,S.-O. and Herschlag,D. (2002) Dissection of a metal-ion-mediated conformational change in Tetrahymena ribozyme catalysis. *RNA*, **8**, 861–872.